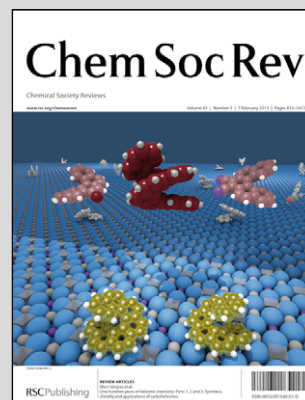Time-Dependent DFT

Featuring works from the groups of Prof. Carlo Adamo and Prof. Denis Jacquemin, at Chimie ParisTech, Université de Nantes and Institut Universitaire de France.

The calculations of excited-state properties with Time-Dependent Density Functional Theory

During the last decade, Time-Dependent Density Functional Theory has become increasingly popular to model excited-states resulting from light-matter interactions. One has now access not only to transition energies, dipole moments and charges, but also to chemically intuitive descriptors.

RSC Publishing

www.rsc.org/chemsocrev

Chem Soc Rev

TUTORIAL REVIEW

The calculations of excited-state properties with Time-Dependent Density Functional Theory

Carlo Adamo[ab] and Denis Jacquemin*[bc]

In this tutorial review, we show how Time-Dependent Density Functional Theory (TD-DFT) has become a popular tool for computing the signatures of electronically excited states, and more specifically, the properties directly related to the optical (absorption and emission) spectra of molecules. We discuss the properties that can be obtained with widely available programs as well as how to account for the environmental effects (solvent and surfaces) and present recent applications in these fields. We next expose the transformation of the TD-DFT results into chemically intuitive parameters (colours as well as charge-transfer distances). Eventually, the non-specialised reader will find a series of advices and warnings necessary to perform her/his first TD-DFT calculations.

Key learning points
★ Properties that can be obtained with TD-DFT
★ Methods to account for environment
★ Schemes to reach colours and charge-transfer
★ Limits of today's TD-DFT models

1. Introduction

Density Functional Theory (DFT) is certainly the most widely applied *ab initio* approach for modelling the ground-state (GS) properties of molecules, clusters and solids.[1] Interestingly this model was originally viewed as unable to describe chemical bonds, but continuous improvements of the exchange–correlation functionals[2,3] – the only approximated term in DFT – allowed DFT to become a blockbuster in both chemistry and physics. To treat electronically excited-states (EESs), that usually results from light-matter interactions, DFT should be extended to account for the time-dependent (TD) nature of the electromagnetic waves. This leads to Time-Dependent Density Functional Theory (TD-DFT) that is an exact solution of the TD Schrödinger equation.[4] Since the emergence of an efficiently implementable formalism,[5,6] TD-DFT has become increasingly popular. For instance, there were "only" 37 TD-DFT publications in 1997 but more than 1000 TD-DFT papers have been published in 2011, and this number has been

steadily increasing during the last fifteen years. As for DFT, this success can be ascribed to both the outstanding accuracy/*cpu*-effort ratio supplied by TD-DFT and to the continuous development efforts made to improve the accuracy and application range of the method.

There already exist one excellent book,[7] and a series of reviews[8–17] treating both mathematical aspects and applications of TD-DFT for (specialised) quantum chemists. In this tutorial review, we present an accessible state-of-the-art in the field. In addition, we also aim to show how the TD-DFT tool can now be used by non-expert users to simulate a series of data in a direct link with experimental measurements. We have therefore willingly limited ourselves to the most popular spectroscopic properties and to give advices and warnings intended to beginners in the field. For this reason, though we show very recent applications, we will not discuss complex cases such as reactivity, multi-reference situations nor EES presenting a doubly-excited nature in the following.

2. Computable properties

2.1 Absorption, emission and adiabatic energies

The different relative EES energies that may constitute the targets of TD-DFT calculations are sketched in Fig. 1. The energy

[a] *Laboratoire LECIME, CNRS UMR-7575, Chimie-ParisTech, 11 rue P. et M. Curie, F-75231 Paris Cedex 05, France*

[b] *Institut Universitaire de France, 103, bd Saint-Michel, F-75005 Paris Cedex 05, France*

[c] *CEISAM, UMR CNRS 6230, BP 92208, Université de Nantes, 2, Rue de la Houssinière, 44322 Nantes Cedex 3, France. E-mail: Denis.Jacquemin@univ-nantes.fr; Tel: +33-2-51-12-55-64*

This journal is © The Royal Society of Chemistry 2013

Chem. Soc. Rev., 2013, **42**, 845–856 | **845**

difference between the EES and the GS determined at the GS geometry corresponds to an idealised (vertical) absorption,

$$E^{\text{vert–abso}} = E^{\text{EES}}(R^{\text{GS}}) - E^{\text{GS}}(R^{\text{GS}}),$$

whereas the same data calculated on the EES geometry correspond to the fluorescence (if the EES is a singlet-state),

$$E^{\text{vert–fluo}} = E^{\text{EES}}(R^{\text{EES}}) - E^{\text{GS}}(R^{\text{EES}})$$

or to the phosphorescence (if the EES is a triplet state). $E^{\text{vert–abso}}$ is, by far, the most commonly computed data in TD-DFT, as it does not require the knowledge of the EES density nor energy gradient. Estimating fluorescence requires access to TD-DFT forces[18,19] in order to optimise the EES geometry (see Section 2.2), and these forces are now available in most DFT codes. Unfortunately, as the experimental processes cannot be viewed as purely vertical, straightforward comparisons of the vertical absorption and/or emission energies with measured longest wavelength of maximal absorption (λ_{max}) is an approximated procedure, despite the huge popularity of this approach. Numerous comparisons between λ_{max} and $E^{\text{vert–abso}}$ are available in the literature and have been discussed in previous reviews (see Introduction), so that there is no need to comment them further.

The adiabatic contribution is simply the difference of energies of the two states in their respective minimum, that is

$$E^{\text{adia}} = E^{\text{EES}}(R^{\text{EES}}) - E^{\text{GS}}(R^{\text{GS}})$$

and is therefore a by-product of a joint absorption/fluorescence calculation. The determination of the 0–0 energies implies calculations of ΔE^{ZPVE}, which is the difference of zero-point vibrational energy between the EES and the GS:

$$\Delta E^{\text{ZPVE}} = E^{\text{ZPVE}}(R^{\text{EES}}) - E^{\text{ZPVE}}(R^{\text{GS}})$$

$$E^{0-0} = E^{\text{adia}} + \Delta E^{\text{ZPVE}}$$

In the vast majority of cases, ΔE^{ZPVE} is negative.[20–23] For typical conjugated organic and inorganic molecules, it lies within the -0.04 to -0.12 eV range, it is therefore a small but non-negligible correction to the adiabatic energies, leading to the 0–0 energies.
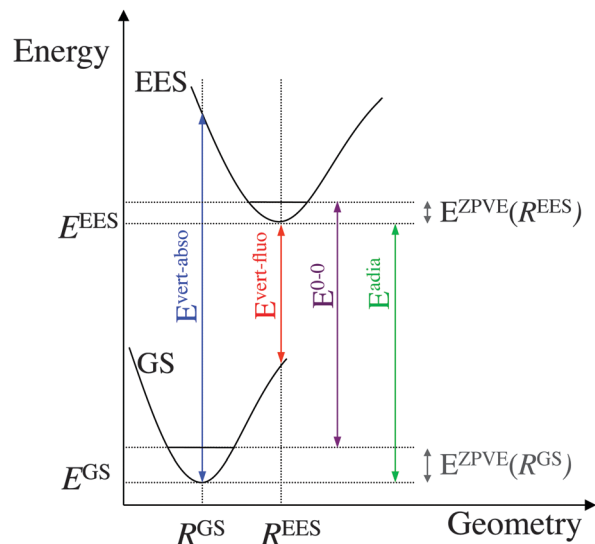

Fig. 1 Simplified Jablonski diagram representing only two singlet states free of intersection(s). Adapted with permissions from D. Jacquemin, A. Planchat, C. Adamo, B. Mennucci, *J. Chem. Theory Comput.*, 2012, **8**, 2359–2372. Copyright 2012, American Chemical Society.

However, determining the vibrational signatures of EES (see Section 2.2) requires TD-DFT second derivatives. Analytic forms of these derivatives have recently been obtained and implemented,[24] but are not yet available in a large set of programs (see Section 6). Therefore, most calculations of E^{0-0} are still performed with ΔE^{ZPVE} obtained through numerical differentiation of the TD-DFT gradients. The advantage of computing the 0–0 energies is that well grounded comparisons with experiments can be made. Indeed, in accurate gas phase experiments, it is often possible to detect the 0–0 bands,[22] whereas for measurements in condensed phase the crossing point between the absorption and fluorescence curves can be used as 0–0 reference[21,23]

The typical errors of TD-DFT for E^{0-0} are below the 0.3 eV threshold, *e.g.* it is 0.24 eV for the molecule at the centre of Fig. 2.

Denis Jacquemin (left) and Carlo Adamo (right)

Carlo Adamo (born 1963) obtained his PhD in Theoretical Chemistry at the University "Federico II" of Naples (1995). Between 1993 and 2000 he was an Assistant Professor at the University of Basilicata (Italy). In 2000, he moved to ENSCP (France) as an Associate Professor where he became a Full Professor in Theoretical Chemistry in 2004. In 2011 he was admitted to the Institute Universitaire de France as a senior member. His main research interests concern the development of new DFT approaches and their application to various fields of chemistry, including those related to energy production.

Denis Jacquemin (born 1974) obtained his PhD, performed under the supervision of Professor André, at the University of Namur (1998). He next moved to University of Florida for a post-doctoral stay with Professor Öhrn in QTP. He came back to Europe, where he was appointed as research associate of the Belgian FNRS (2003) and next Professor at the University of Nantes (2010). He obtained an ERC starting grant (2011) and he is a junior member of the Institut Universitaire de France (2012). His research interests are focused on modeling the electronically excited-states in dyes and photochromes.
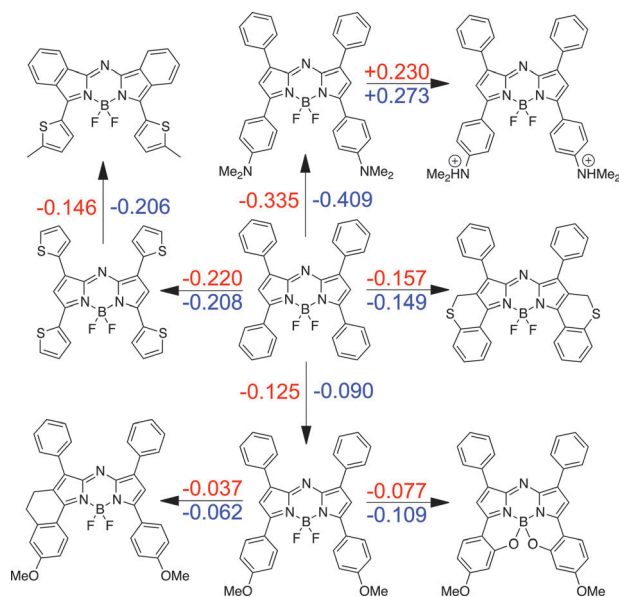
Fig. 2 Comparison between experimental (red) and TD-DFT (blue) auxochromic shifts for E^{0-0} in a series of aza-BODIPY structures. All values are in eV. Original [SS-PCM-TD-BMK] data can be found in ref. 25.

Fig. 3 Comparison between GS (left) and EES (right) geometries of diphenyl-acetylene (**I**) and biphenyl (**II**). Central distances (in Å) are also given [calculations at the PCM-CAM-B3LYP/6-31+G(d) level of theory].

However, one is generally interested in relative data in a series of similar molecules that is one often aims at determining auxochromic (acidochromic, solvatochrmoic...) effects rather than at determining absolute energies. In that case, the errors provided by TD-DFT tend to be significantly smaller, especially when a series of structurally related molecules are considered. This is illustrated in Fig. 2 for a series of well-known fluorophores.[25] For the eight proposed structural variations, the mean absolute TD-DFT deviation is as small as 0.036 eV, the largest error being limited to 0.074 eV. This illustrates how TD-DFT is indeed efficient in the dye design line of research.

2.2 Geometries and vibrational frequencies

TD-DFT allows one to determine the optimal geometries of EESs, which is particularly useful to analyse fluorescence, as the experimental determination of EES bond lengths and valence angles remains, at best, very challenging for molecules. Large (small) differences between the GS and EES geometries are generally associated with important (limited) Stokes shifts (the difference between emission and absorption energies), and TD-DFT is a convenient approach to rationalise these shifts. In addition, theory is able to foresee conformational changes (*e.g.* H-bond formation) at the EES and therefore to provide hints in more complex situations.

For diphenylacetylene, comparisons between GS and EES structures can be found in Fig. 3. For this aromatic derivative, the two geometries are qualitatively similar, but the central bond lengths significantly differ. Indeed, in the GS, the bond length alternation (BLA, the difference between single and triple bond lengths) attains 0.221 Å, a value divided by two upon electronic transitions (0.109 Å), which indicates a sizeable improvement of the electronic delocalisation along the π-backbone. In contrast, the C–H σ bonds that are not part of the conjugated system remain almost
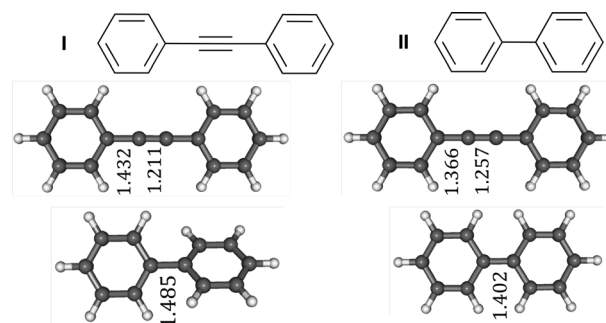
unchanged when going from GS to EES (1.085 ± 0.001 Å). The characteristic vibrational mode corresponding to the simultaneous elongation/contraction of the triple/single bond – the so-called effective conjugation coordinate (ECC) mode – is significantly modified when changing states. Indeed, it is located at 2358 cm^{-1} for the GS but 2193 cm^{-1} for the EES. In the same time, the variation of the vibrational frequency corresponds to the simultaneous and symmetric stretching of the ten C–H bonds varies by less than 1 cm^{-1} upon electronic transition.

Consistently with the relatively limited structural deformation, **I** presents a relatively small Stokes shift (700 cm^{-1}), which contrasts with biphenyl, **II**, that becomes planar upon transition (the central twisting angle goes from *ca.* 38° at the GS to zero at the EES) and undergoes a Stokes shift one order of magnitude larger, an effect qualitatively reproduced by TD-DFT.

2.3 Vibronic couplings

If the GS and EES vibrational signatures are known (see above), it is possible to compute vibrationally resolved optical spectra thanks to the determination of coupling factors within the Franck–Condon (for strongly dipole allowed transitions) and/or Herzberg–Teller (for forbidden or weakly allowed transitions) approximations.[20,26] These vibronic calculations, often performed on the basis of harmonic frequencies, therefore provide shapes of absorption and emission bands that can be directly compared to measurements.

For diphenylacetylene, a comparison between experimental and theoretical band shapes is provided in Fig. 4, for which we have used unscaled harmonic frequencies. For absorption, the agreement is extremely satisfying, as the position and height of all main peaks is restored, but for an underestimated 0–0 intensity. The most intense band appearing at *ca.* 2200 cm^{-1} above the 0–0 transition, corresponds to the 2193 cm^{-1} EEC mode discussed previously. This result is not surprising: this vibration corresponds to the variation of the bond lengths in the central moiety, which could be seen as a connecting displacement between the GS and EES structures of Fig. 3. However, in larger less symmetric molecules, intuition might become misleading for analysing/predicting vibronic couplings, as they tend to result for complex combinations of low-frequency deformations.[26,27] For the emission band, the agreement between theoretical simulations and
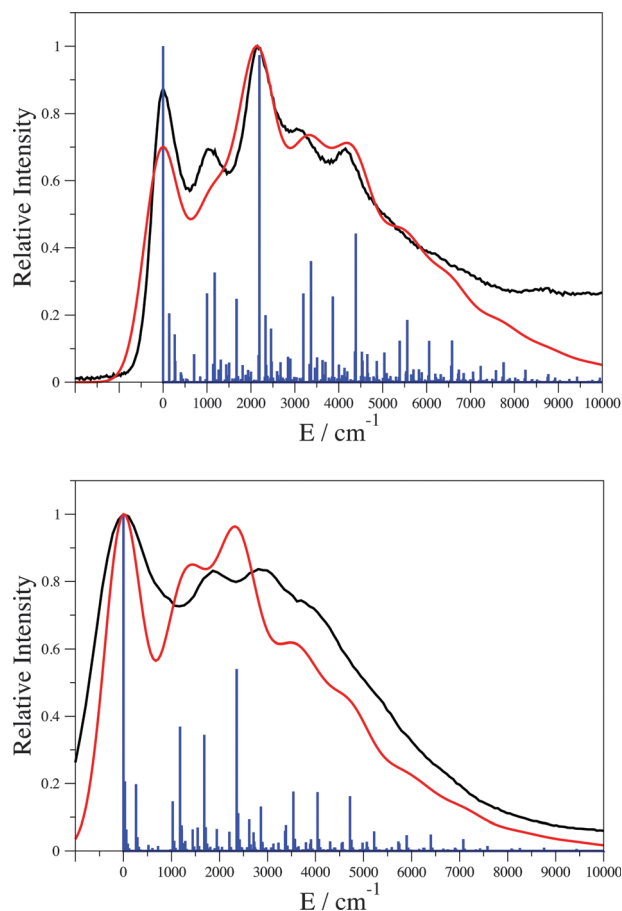
Fig. 4 Comparison between experimental (black lines) and theoretical (red lines for convolution of the blue sticks) band shapes for **I**. Top: absorption, bottom: emission, in both cases the energy of the 0–0 transition was set to zero to allow direct comparisons. See caption of Fig. 3 for more details.

Fig. 5 Middle: GS and EES dipole moments (red vector) for the DPP dye represented at the top. Their norms are 5.31 D (GS) and 8.24 D (EES). Bottom: total charges borne by several moieties of the molecule [CAM-B3LYP/6-31+G(d) calculations, Merz–Kollman atomic point charge model].

conversion. We underline that for non-substituted BODIPY (see Section 3.1), the GS and EES dipole moments are almost equal: 4.43 D for the former and 4.22 D for the latter, illustrating that the nature of the electronic transition strongly differs in **III** and **IV**.

3. Environmental effects

The EES properties tend to be more environmental-dependent than their GS counterparts and completely neglecting the impact of the surroundings during TD-DFT calculations is seldom a pertinent choice. Therefore, it is essential to grasp the key ideas for mimicking the interplay between EES and their environment (solvent, cage, surface, protein...). Except for micro-solvated structures that can be fully computed at the TD-DFT level, the model is split into two parts: the chromophoric group that absorbs/emits light and is simulated with TD-DFT, and the environment treated at a simplified level of theory.

Irrespective of the type of surrounding, correctly reproducing the response of the environment to the electronic transition of the chromogen is the key to success. One can distinguish two reaction limits: the non-equilibrium and the equilibrium interaction modes. In the former, only the electrons of the medium do adapt to the EES of the chromophore, and the effective dielectric constant of the environment interacting with the new electronic state is the square of the refraction index of the medium (*ca.* 2 in most cases). In the latter, a full relaxation of the environment (both electrons and nuclei) is allowed and the effective dielectric constant corresponds to the static limit, as for GS properties (*e.g. ca.* 78 for water). In general, vertical transitions are so fast that they should be computed within the non-equilibrium limit, whereas geometry optimisations of the EES better correspond to an equilibrium situation. Therefore, the energies listed above can be computed as,

experiments remains valuable but is probably less impressive as the positions of the second and third maxima are both underestimated (see bottom of Fig. 4).

2.4 Dipole moments and atomic point charges

In addition, one can also determine partial atomic charges, dipole moments and electron densities with TD-DFT. This allows us to estimate variations of the polarisation of the molecule once photon has been absorbed, but also to mimic charge transfer states (see Section 4.2). Nevertheless, in contrast to GS DFT calculations, these figures are not direct by-product of energy calculations but require a supplementary computational effort, similar to the determination of TD-DFT forces.

Such calculations are illustrated in Fig. 5 for a diketopyrrolo-pyrrole (DPP) molecule that has a potential for applications as dye in dye-sensitised solar cells. Clearly, one notices that photon absorption induces a large increase of the dipole moment (+2.95 D) and a change of orientation of the dipole towards the anchoring group. Concomitantly, a quite limited increase of the electronic charge borne by the terminal cyano-acetic group and a decrease of the charge of the DPP moiety are noticed. These characteristics are favourable for solar-to-electricity
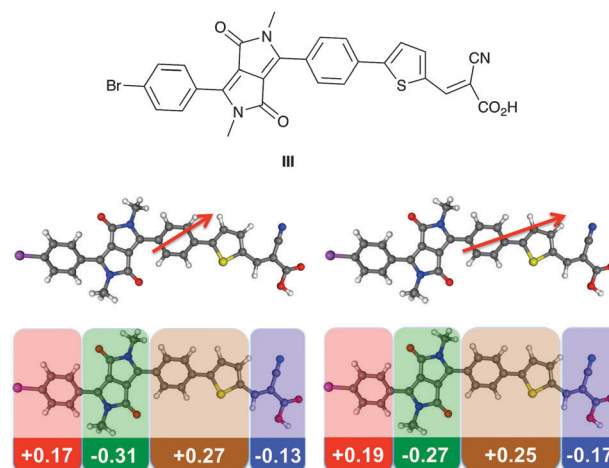
848 | *Chem. Soc. Rev.*, 2013, **42**, 845–856

This journal is © The Royal Society of Chemistry 2013

$$E^{\text{vert}-\text{abso}}(\text{neq}) = E^{\text{EES}}(R^{\text{GS}}, \text{neq}) - E^{\text{GS}}(R^{\text{GS}}, \text{eq})$$

$$E^{\text{vert}-\text{fluo}}(\text{neq}) = E^{\text{EES}}(R^{\text{EES}}, \text{eq}) - E^{\text{GS}}(R^{\text{EES}}, \text{neq})$$

$$E^{\text{adia}}(\text{eq}) = E^{\text{EES}}(R^{\text{EES}}, \text{eq}) - E^{\text{GS}}(R^{\text{GS}}, \text{eq})$$

$$E^{0-0}(\text{eq}) = E^{\text{adia}}(\text{eq}) + \Delta E^{\text{ZPVE}}(\text{eq})$$

Note that for absorption, the solvent is in equilibrium with the GS but in non-equilibrium with the EES, the reverse situation appearing for emission. We also underline that, by definition, adiabatic and 0–0 energies do correspond to the equilibrium limit. Therefore, though it is legitimate to compare 0–0 energies to the experimental absorption/fluorescence crossing point for gas-phase simulations, such comparisons require a correction for non-equilibrium effects in condensed phase. We redirect the interested reader to ref. 23 for a longer discussion of this topic.

3.1 Bulk solvation

Amongst all possible media, solvated molecules have attracted the largest efforts. There exist two main approaches to estimate solvent effects: explicit and implicit models. In the former, all molecules of the environment are explicitly treated, usually with a molecular mechanics approach, which provides a complete description but remains often computationally challenging. Indeed, there exist many possible spatial arrangements for the solvent molecules, and primary dynamical steps followed by several TD-DFT calculations performed on snapshots could be necessary.[28] In the latter, the entire environment is treated as a structureless continuum presenting the same macroscopic properties as the actual solvent, one of the most well-known schemes in this category being the Polarisable Continuum Model (PCM).[29] Though continuum schemes lack a description of the specific solute–solvent interactions (e.g. hydrogen bonds, ion pairing, π-interactions...), they present the advantage to allow estimating media effects for a relatively limited computational cost. However, in continuum models, the solute–solvent border needs to be correctly polarised. During TD-DFT calculations, the interactions of this polarisation with the electronic transition may be accounted with different levels of refinement. The most common model – the so-called linear-response (LR)[29] scheme – provides a first order approximation than can be improved by using corrected linear-response (cLR)[30] or state-specific (SS) approaches,[31] the former (latter) being based on a perturbative (self-consistent) scheme. Methodological details and future discussion regarding these models may be found in ref. 17 and references therein.

Comparisons between vertical transition energies computed for the two molecules of Fig. 6 with different models can be found in Table 1. For absorption, the solvatochromic shifts
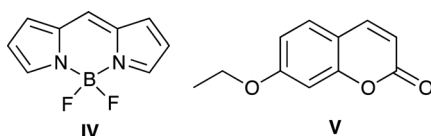
Table 1 Gas phase transition energies and solvent shifts (water) evaluated with several PCM approaches combined to TD-DFT for the two molecules sketched in Fig. 6. All [PBE0/6-31+G(d)] values in eV

| | Transition | Gas | Solvatochromic shifts | | | |
			(LR, eq)	(LR, neq)	(SS, eq)	(SS, neq)
IV	$E^{\text{vert}-\text{abso}}$	3.16	−0.39	−0.11	0.00	+0.02
	$E^{\text{vert}-\text{fluo}}$	2.93	−0.24		+0.14	+0.13
V	$E^{\text{vert}-\text{abso}}$	4.17	−0.29	−0.12	−0.34	−0.16
	$E^{\text{vert}-\text{fluo}}$	3.78	−0.27		−0.12	−0.15

are significantly larger in the equilibrium limit than in the non-equilibrium limit, which is the usual outcome for a $\pi \rightarrow \pi^{\star}$ in a polar medium: the equilibrium limit allowing an extra stabilisation of the EES compared to the non-equilibrium limit and hence a decrease of the transition energy. While the SS and LR values are quite comparable for the absorption of the coumarin, **V**, they significantly differ for the BODIPY, **IV**, and this is also true for emission, the LR model significantly overestimating the positive solvatochromism. At least for the emission, the selection of advanced solvation models is often required.

3.2 Complex environment

Beyond solvent effects, molecular photo-physical properties can be tuned by more complex chemical environments such as organic cages, protein and surfaces. Following a kind of analogy with solvent effects, such complex environments can act in a specific and non-specific way. In the first case, the environment is directly involved in the electronic excitation which, for instance could correspond to charge transfer from an orbital localised on the dye into an orbital belonging to the environment. In such a case both moieties should be treated within the same Hamiltonian, thus requiring an increased computational effort.

Non-specific interactions can be treated in a different way since their role is to polarise to some extend the electronic density of the excited molecules, thus shifting the associated optical spectra to lower or higher energies, depending on the considered compounds. This is the case, for instance, of a dye encapsulated in an organic cage, in interaction with an ADN chain or absorbed over a surface. In all these cases, the chromophore could either covalently bound to the chemical environment or in weak interaction (such as dispersion interaction or H-bond) with it, but the electronic excitations are still localised only on the chromophore itself. In other words no charge transfer takes place. As in the case of solvent, the effect of the surrounding is twofold: direct and indirect. The direct is limited to the polarisation of the electron density of the chromophore, while the indirect is related to the structural modifications induced by its interaction with the environment. As long as the excitation can be considered as localised on the chromophore, an effective approach is based on a divide-et-impera (divide-and-conquer) strategy where the two subparts (dye and surrounding) are treated with different models. In other words the dye can be treated using a TD-DFT approach (with any kind of exchange–correlation functional) and the rest either with another quantum mechanics method (such as DFT, HF or semiempirical) or with molecular mechanics (typically using standard force fields like AMBER or UFF). In such a way

Fig. 6 BODIPY core (left) and 7-OEt-coumarin (right).

QM/QM or QM/MM models are generated. Then the indirect effects are straightforwardly included in any model considering a mechanical embedding that is the structural constrains of the surrounding on the dye geometry. However direct effects are taken into account only if the two model levels (QM and QM or QM and MM) are coupled through an electronic term. Indeed the perturbation induced by the environment should be added, using appropriate terms and approximations, in the Hamiltonian of the dye. This is done in a more rigorous way at the QM level so that most of the QM/MM models could be ineffective, including only the mechanical embedding, and should be discharged.

Among the different QM/QM approaches available the so-called ONIOM (our Own N-layered Integrated molecular Orbital) is particularly intuitive to use and it has been shown to be very effective.[32] This multi-layered method combines different theoretical approaches (typically a low and high level) for describing the real large system (at low level) and its part of interest (at both low and high levels). An extrapolation procedure is then applied. The original approach takes into account only mechanical embedding, whereas recent advances include electronic embedding, which includes an electronic coupling term in the high level model extracted from the low level.[33] More details about embedding schemes for an excited-state can be found in a recent review.[34]

An illustrative example is represented by β-carotene, a natural pigment with high potential for photonic applications, trapped in a single wall carbon nanotube (SWCNT, see Fig. 7). Encapsulation prevents its degradation, but blue shifts its absorption energy by 0.24 eV (from 466 nm in DMF to 512 nm in SWCNT). Here, the multi-layer approach used considered a range-separated hybrid TD-DFT approach as high theoretical level and a DFT scheme with dispersion interactions as low level. Electronic embedding is then added considering an electrostatic coupling between the two levels. The combination of these different models within an ONIOM scheme allows us to take into account simultaneously the β-carotene spectral features, the dispersion forces ruling the structural rearrangement and the confinement effects. The theoretical spectra, plotted in Fig. 8, are shifted by *ca.* 50 nm with respect to the experimental ones, but the variation observed when going from the solution to the SWCNT is well reproduced (0.22 eV). A detailed analysis of the theoretical results suggests that this shift is due, on the
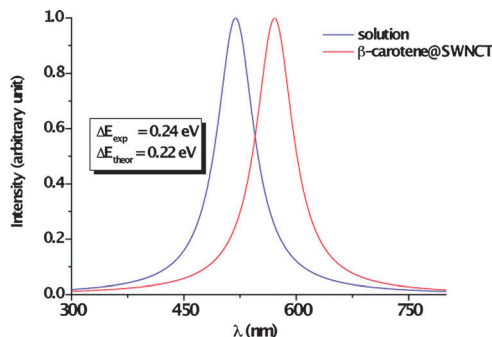

Fig. 8 Theoretical spectra computed for β-carotene in (12,8) SWNCT and in DMF solution. Original data in G. Moreno, I. Ciofini, M. Fernndez–Gomez, C. Adamo, submitted.

one hand, to the polarisation effects induced by the confinement and, on the other hand, to structural rearrangement. Indeed only the s-*cis* isomer of the β-carotene is found inside the SWCNT, in agreement with experimental evidence. This example, as well others on dyes embedded in organic cages, in protein or adsorbed on surfaces,[35,36] well illustrates the accuracy of such composite methods where modern TD-DFT approaches are coupled with effective environment descriptions.

4. Towards chemically intuitive quantities

4.1 Colours

The absorption of one photon in the visible domain of the electromagnetic spectrum by a chromophore induces not only an electronic transition towards an EES, but also modifies the panel of wavelengths present in the reflected or transmitted light. Consequently the so-called *chemical colours* are one of the most common and industrially relevant applications of EES. To reach a valuable description of the physiologically perceived colours from TD-DFT calculations,[27,37] one first needs a very accurate description of the shape of the absorption spectrum (see below for an illustrative example). Once this requirement is fulfilled, it is possible to transform these *ab initio* spectra into colourimetric parameters with a relatively straightforward procedure:

1. Determine the nature of the outgoing light, that, for a solvated dye, corresponds to the transmittance spectra, $T(\lambda)$, *i.e.* is proportional to the inverse of the absorption spectra in the visible domain.

2. Calculate the tristimuli functions in the *XYZ* colour basis using:

$$X = k \int P(\lambda)T(\lambda)x(\lambda)$$

$$Y = k \int P(\lambda)T(\lambda)y(\lambda)$$

$$Z = k \int P(\lambda)T(\lambda)z(\lambda)$$

where k is a normalisation factor, $P(\lambda)$ is the spectral power of the illuminant and $x(\lambda)$, $y(\lambda)$ and $z(\lambda)$ are colour matching functions corresponding to the responses of the standard human
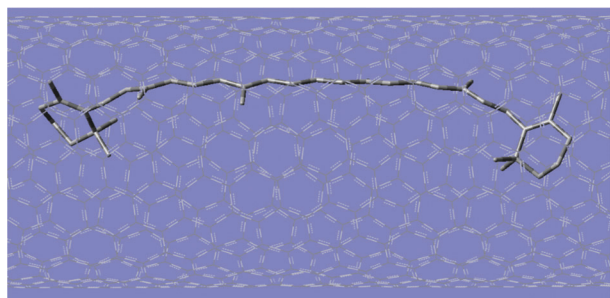

Fig. 7 Structure of β-carotene in (12,8) SWNCT. The system has been fully optimised using an ONIOM approach (PBE0/6-31+G//PBE+D/STO-3G) including electronic embedding. Original data in G. Moreno, I. Ciofini, M. Fernndez–Gomez, C. Adamo, submitted.
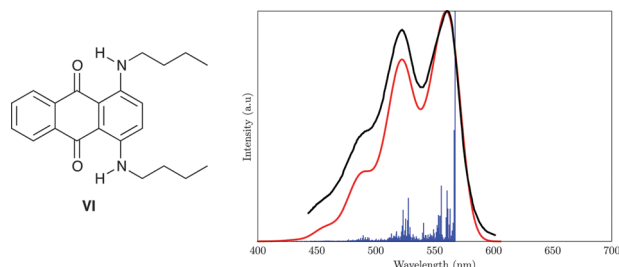
Fig. 9 SB35 (left) and comparison between experimental (black) and theoretical (blue sticks and red line) absorption spectra for the visible band of this dye. An offset of 0.33 eV has been used for the theoretical curve so to allow direct comparisons of band shapes. Adapted with permissions from D. Jacquemin, E. Brémond, I. Ciofini, C. Adamo, *J. Phys. Chem. Lett.*, 2012, **3**, 468–471. Copyright 2012, American Chemical Society.

Table 2 Experimental and theoretical colours for **VI**.[27] These data correspond to Fig. 9

Experiment	Theory (vibronic)	Theory (no vibronic)

eye to red, green and blue stimuli, respectively. These functions have been tabulated,[38] and the same holds for the spectra of common light sources.

3. Once the *XYZ* parameters have been calculated, straightforward algebraic transformations allow to obtain colourimetric parameters in well-known spaces, such as RGB or HSV. We advocate the use of the CIE *L*a*b** model that is anthropocentric: the Cartesian distance, in the CIE *L*a*b** sphere, between two colours is (almost linearly) proportional to the perceived variation.

In practice, one can determine the colour of the dye under several conditions (*e.g.* daylight *versus* mercury lamp illuminants), the accuracy of the predicted colour depending only on the quality of the TD-DFT results.

Solvent blue 35 (SB35, **VI** see Fig. 9) is an anthraquinoidic dye, which, as his name implies, appears blue in most media. It presents a structured band due to vibronic effects. As can be seen in Fig. 9, TD-DFT is able to reproduce very satisfactorily the experimental band shape once vibrational couplings are accounted for. Following these calculations, a transformation into colour coordinates was performed. Selected results are displayed in Table 2, and clearly illustrate the sensitivity of the human eye. Indeed, by switching off the coupling between electronic and vibrational effects, that is by considering a single peak rather than a multi-maxima topology of the absorption band, **VI** becomes a yellow dye. In the same vein, though the experimental and theoretical spectra show almost perfect match, one can perceive colour difference in Table 2. Such calculations are not only useful to allow direct comparisons with the experimental pot, they additionally pave the way to the fine tuning of the colours by changing auxochromes that influence the band shapes rather than the position of the λ_{max}.

4.2   Charge-transfer

Through-space charge transfer (that we simply abbreviate as CT in the following) EESs play a key role in many technological applications including solar-to-electricity conversion devices, light emitting diodes and both natural and artificial photosynthetic architectures. Indeed, CT states correspond to a light-activated electron–hole separation where the positive and negative charges are distant enough to allow their independent collection. In order to maximise CT, an efficient molecular strategy is to design push–pull rod-like compounds. In these systems, an electron-donor (D) and an electron–acceptor (A) are located at the extremities of a quasilinear conjugated spacer. In this way, one formally goes from a D–π–A GS to a D$^+$–π–A$^-$ EES. However, a rational optimisation is uneasy as CT often remains a fuzzy concept. In that framework, TD-DFT calculations are certainly helpful. Indeed, one can determine the electronic density of the ES (see above), the corresponding GS density being obtained through standard DFT calculations. Starting with these two densities, $\rho^{\text{ES}}(r)$ and $\rho^{\text{GS}}(r)$, respectively, one can compute a CT distance (expressed in units of length) in four successive steps:[39]

1. Compute the electronic density difference between the two states,

$$\Delta\rho(r) = \rho^{\text{ES}}(r) - \rho^{\text{GS}}(r).$$

2. Separate regions of electronic density increase/decrease upon photon absorption. For the positive domain, this yields,

$$\rho^+(r) = \begin{cases} \Delta\rho(r) & \text{if } \Delta\rho(r) > 0 \\ 0 & \text{if } \Delta\rho(r) < 0 \end{cases},$$

and similarly to $\rho^-(r)$.

3. Determine the barycenters of both regions, *e.g.* for the positive side,

$$r^+ = N\int r\rho^+(r)\mathrm{d}r.$$

4. Calculate the CT distance as the separation between r^+ and r^-:

$$d^{\text{CT}} = |r^+ - r^-|.$$

These four stages are illustrated for a typical triphenylamine dye in Fig. 10. Note that in addition to a CT distance, d^{CT}, the amount of transferred charge, q^{CT}, is obtained by integrating $\rho^+(r)$ over space. This dipolar approach allows one to compare different molecules on a perfectly equal footing, the only "approximation" being the nature of the selected method (functional and basis set, see Sections 5 and 6).

Recently, this methodology was applied to simulate a large set of push–pull molecules used in dye-sensitised solar cells.[40] For a given D/A pair, a study of the evolution of d^{CT} as a function of the length of the central spacer produces a bell-shaped curve. Indeed short systems are limited by the lack of π-conjugation, whereas in extended systems, one notices either that the accepting group extracts the electron from the bridge rather than from the donor (see Fig. 11 for a typical illustration) or that the lowest-lying EES recovers the local and symmetric nature of the bare π-spacer.
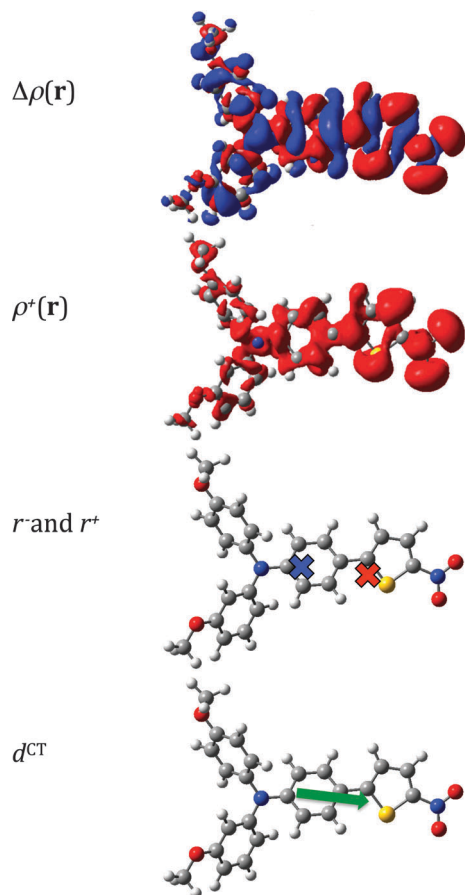
Fig. 10 Illustration of the four steps of the computation of the CT distance. Red (blue) regions indicate an increase (decrease) of electron density upon electronic transition. Top figure reproduces with permissions from I. Ciofini, T. Le Bahers, C. Adamo, F. Odobel, D. Jacquemin, *J. Phys. Chem. C*, 2012, **116**, 11946–11955. Copyright 2012, American Chemical Society.
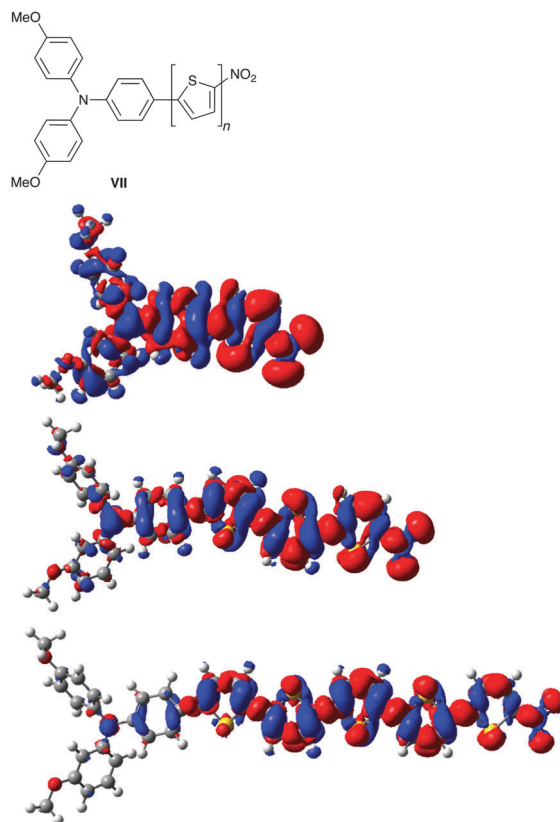

Fig. 11 Top: sketch of the push–pull structure. Bottom: density difference plots for the chains containing *n* = 1, 3 and 5 thiophene rings. The computed d^{CT} are 3.82 Å, 4.56 Å and 4.32 Å, for the monomer, trimer and pentamer, respectively. Adapted with permissions from I. Ciofini, T. Le Bahers, C. Adamo, F. Odobel, D. Jacquemin, *J. Phys. Chem. C*, 2012, **116**, 11946–11955. Copyright 2012, American Chemical Society.

For typical push–pull systems, the maximal CT is reached for 3–5 connecting rings between the electroactive groups. The most effective acceptor groups are able to induce a CT exceeding 5 Å with a pentathiophene spacer. TD-DFT has allowed us to substantiate that increasing the strength of the terminal electro-active groups or improving the delocalisability by adding more π-electrons in the bridge does not systematically improves the CT properties. As d^{CT} is shorter than the distance between the donor and the acceptor moieties, TD-DFT can obviously provide rational insights to drive the synthetic efforts towards the most efficient CT dyes.

5. Pitfalls

In this section, we list several significant limitations encountered with TD-DFT. Nevertheless, we emphasise that as TD-DFT is, in principle, an exact theory, these deficiencies are related to the limits of today's implementations and developments rather than to errors in the formal theory.

5.1 Long-range charge-transfer

It is known since 15 years that standard DFT functionals, *e.g.* B3LYP, suffer from an over-polarisation problem.[41] In simple terms, when a charge separation appears, the electron and the hole do not properly interact. In the TD-DFT framework, this leads to both spurious CT states (CT states that have no physical meaning)[42,43] as well as large errors in actual CT transition energies.[42,44] In addition the magnitude of the errors tends to increase with the size of the considered system. These problems have been exemplified by the zincbacteriochlorin–bacteriochlorin dyad: deviations can be as large as 2 eV with some functionals.[42] To solve this problem, one can use range-separated hybrids (RSH) functionals,[44–46] that include a non-constant percentage of Hartree–Fock like exchange. RSH often provides an accurate interaction between the electron and its hole, irrespective of the separation distance, therefore allowing us to recover qualitatively correct evolutions. However, when very strong CT effects take place, it may be mandatory to change the parameters of the RSH to reach valuable transition energies and excited-state dipoles.[47,48] For the zincbacterio-chlorin–bacteriochlorin dyad, the use of an adequate RSH lifts the previously mentioned difficulties.[49] In that framework, Tozer and coworkers proposed an elegant and efficient test (so-called Λ diagnostic) that allows us to qualitatively check when the use of RSH becomes mandatory,[44] but other criteria have been proposed in the literature.[39,50]

852 | *Chem. Soc. Rev.*, 2013, **42**, 845–856

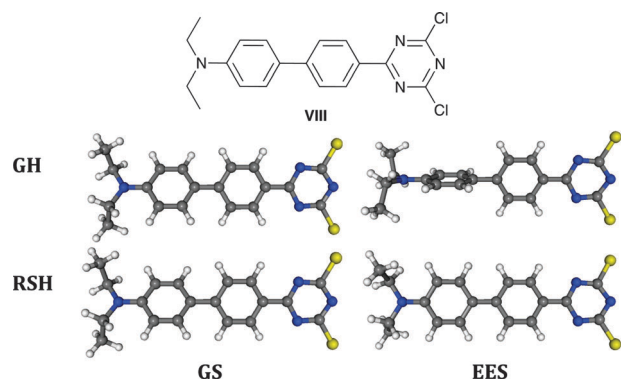This journal is © The Royal Society of Chemistry 2013

Fig. 12 Calculated structures for the ground (left) and first excited-(right) states for the compound shown at the top. Middle: results obtained with a global hybrid functional (GH, B3LYP), bottom: range-separated hybrid (RSH, CAM-B3LYP) geometries. Adapted with permissions from D. Jacquemin, A. Planchat, C. Adamo, B. Mennucci, *J. Chem. Theory Comput.*, 2012, **8**, 2359–2372. Copyright 2012, American Chemical Society.

5.2 Potential energy surfaces

Related to the CT transition energy problem discussed in the previous section, TD-DFT optimisations might lead to qualitatively incorrect results in some cases. This problem was originally pointed out by Tozer's group for the model 4-(dimethylamino)-benzonitrile structure: usual functionals provide a twisted excited-state geometry with the NMe_2 donor group perpendicular to the central phenyl ring, a prediction denied by higher levels of theory.[51] As for CT transition energies, the use of RSH allows one to cure the problem.[51] Since that time, other examples appeared in the literature,[23,52] one of which is displayed in Fig. 12.[23] As can be seen, though the GS optimal geometries are rather independent of the selected DFT model with a dihedral angle between the two central rings, τ, of *ca.* 30°, the EES structures differ with a realistic planarisation with the RSH (τ of 14°) but an incorrect perpendicular EES with B3LYP. Such an error of B3LYP might lead to misinterpretation of experimental facts, *e.g.* one could incorrectly assign two peaks in an emission spectrum to the presence of both a planar and a twisted intramolecular CT state (PICT and TICT), whereas vibronic couplings better explain the experimental band shapes.[53] Obviously, this might also leads to difficulties when simulating photochemical reactions with TD-DFT.

5.3 Non-Franck–Condon transitions

In most cases, one assumes that experimental measurements correspond to vertical transitions. This is not always true, and has led to a long-standing TD-DFT problem: the calculation of
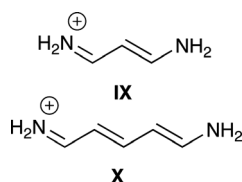

Fig. 13 Sketch of two classical cyanine dyes. Their experimental λ_{max} are 286 (**IX**) and 378 (**X**) nm in water.

the λ_{max} of cyanine dyes. It can be illustrated with two simple dyes sketched in Fig. 13. The experimental λ_{max} are 4.3 and 3.3 eV for **IX** (C3) and **X** (C5) respectively. Vertical TD-DFT apparently provides very incoherent estimates, typically 1 eV above the experimental values, irrespective of the computational details (functionals, basis sets, inclusion or not of environmental effects...). Recently, Filippi and coworkers performed quantum Monte-Carlo calculations[54] which led to vertical transition energies of 5.03 eV (**IX**) and 3.83 eV (**X**). Selecting these highly-accurate theoretical values as references, it was found that most hybrid functionals provide transition energies with an error smaller than 0.30 eV.[55] In short, in cyanines the measured λ_{max} correspond to processes significantly deviating from an idealized verticality.[54,55] More generally for cyanine-like transitions present in many chromogens relevant for practical applications (BODIPY, tri-arylcarbonium...), one should avoid straightforward comparisons between experimental λ_{max} and vertical TD-DFT values.

5.4 Singlet–triplet transitions

The evaluation of singlet–triplet splittings might be difficult. Indeed, they are much more sensitive to the exact mathematical form of the functional than singlet–singlet transition energies. This outcome has been analysed as related to the GS instability problem.[56] In that framework, the use of the Tamm–Dancoff approximation (TDA, a simplification of the TD-DFT method, implemented in many codes) allows one to circumvent the *triplet problem*. One should nevertheless underline that most singlet EES computed within the TDA approximation tend to be less accurate than their TD-DFT counterpart.

6. Hands on: first-time advices

There exist several free or commercial codes (non-exhaustive alphabetic list: ADF, Dalton, Gamess, Gaussian, NWChem, Octopus, Orca, Q-Chem, Turbomole, Yambo), to perform TD-DFT calculations of transition energies, gradients and densities both in gas and in condensed phases, using continuum models for the latter. Below, is a short FAQ intended to beginners.

What is doable?

Vertical TD-DFT simulations on organic compounds containing up to *ca.* 2000 electrons/400 atoms can be performed with most programs within a (human) week on a modern computing architecture. Each step of a TD-DFT geometry optimisation nowadays costs about twice the *cpu* time necessary for the corresponding vertical calculation. As the potential energy surfaces of the EES tend to be rather flat, optimisation often requires more steps than for GS, limiting the size of the treatable systems to *ca.* 150 atoms. Vibrational signatures that typically imply numerical derivative are often more costly and molecules encompassing more than 100 atoms would require a dramatic cpu effort. Of course, the exact timings and requirements depend on the calculation parameters, selected algorithms and available resources, but in all cases, they tend to rapidly increase with the number of excited-states that are simultaneously

computed. For solvent effects, LR-PCM calculations are nearly as fast as gas phase simulations, whereas cLR-PCM and SS-PCM models imply increase of the computational effort by approximatively a factor of three and ten, respectively.

How to select a relevant atomic basis set?

One should first ascertain that the basis set is adequate for ground-state properties (e.g. one could check that geometrical parameters are sufficiently accurate compared to available XRD data), a necessary but insufficient condition. Indeed, obtaining basis set converged transition energies generally necessitates a specific selection of the basis set. For well-behaved valence excitations, a Pople triple-ζ basis set, ideally including diffuse functions, is often a pertinent choice. In contrast, Rydberg EES can only be rigorously described with much larger basis sets (e.g. aug-cc-pVTZ is a minimum and optimization of the basis set might be necessary), whereas for CT states diffuse orbitals are mandatory, and 6-31+G(d) could be a good selection for relatively rapid yet meaningful calculations. In addition, rather large basis might also be necessary for TD-DFT optimisations, because EES surfaces could be flatter than their GS counterparts.

Which functional to choose?

Plethora of TD-DFT benchmarks are available for both vertical[44,57,58] and adiabatic energies.[21–23] At least one general advice emerged: one should avoid applying pure (i.e. exact-exchange free) functionals as they tend to significantly undershoot the transition energies in the majority of organic and inorganic systems. Go for hybrids: transition energies will be closer to the experimental spot, with an expected error range of 0.20–0.25 eV. For both local $n \to \pi^\star$ and $\pi \to \pi^\star$ states, global hybrids such as B3LYP, PBE0 or M06 will generally provide accurate estimates whereas for CT or Rydberg EES, it is mandatory to use range-separated hybrids (we recommend CAM-B3LYP or ωB97X-D) to reach physically meaningful estimates. These latter functionals also circumvent the main problems when optimising the EES geometries having a strong CT character.

How to analyse the results?

Vertical TD-DFT calculations typically yield the transition energies, the oscillator strengths as well as the molecular orbital (MO) compositions corresponding to each excited-state. Whilst the former are self-explanatory, the second can be related to experimental molar absorption coefficients, and thus to the intensities of the measured absorption bands. The last information allows a chemical interpretation of the results that is, one could relate the EES to a transition between given MO. For the lowest-lying excited states, it is not uncommon that a single occupied/virtual MO pair satisfactorily represents the transition to the EES. However, in the majority of cases, a complex orbital mix is provided by TD-DFT, making analysis cumbersome. There exist two common alternatives bypassing the MO picture: natural transition orbitals (NTO),[59] and calculation of density differences, $\Delta\rho(r)$ (see Section 4.2). These two schemes often provide a more convenient representation of the electronic process.

Troubleshooting

When optimising the structure of excited-states, there is generally no difficulty when one focusses on the first EES. However, geometry optimisations of higher-lying EES might induce crossing with a lower EES during the minimisation procedure. Therefore, one needs to carefully inspect the evolution of the EES to ensure that the starting and ending states have the same chemical nature. Likewise, one should be cautious that the symmetry of the EES and the GS might be different, so that enforcing the GS point group on the EES cannot be done blindly. During numerical vibrational calculations, we recommend checking that the (TD-)DFT integration grid is sufficient to provide accurate values. Depending on the selected programs, the default DFT grid might be too loose. Eventually, one needs to be cautious that environmental models have not uniform defaults throughout the programs. It is often required to verify if the calculations are performed within equilibrium or non-equilibrium limits.

7. Conclusions and outlook

Electronically excited-states play an ubiquitous role in the development of new technologies. As the EES behaves different from ground-states, designing molecules with specific EES features remains a challenge. In that research line, theoretical tools are particularly useful as they can bring, for relatively moderate cost, informations and insights that are difficult to obtain by experimental means, e.g. structural parameters of EES are much more challenging to measure than their GS counterparts. In this tutorial review, we have strived to show that TD-DFT, in spite of its current limits, occupies a favourable spot on that scene. If the modelling of biological environment or the calculation of vibrationally resolved spectra still requires effort and expertise, the computation of absorption and emission signatures can now be performed routinely for most organic and inorganic molecules of interest.

Though TD-DFT is already a powerful and widely-used method, several started developments (will) allow pushing further forwards its limits. These developments span from the design of new exchange–correlation functionals especially suitable for excited states description, to inclusion of complex phenomena in the TD-DFT formalism, like double excitations or non-adiabatic effects. These aspects have been recently summarised in a review.[60] On top of all these improvements, the description of the excited state behaviour in more complex environments using more sophisticated embedding techniques will allow, in a close future, for accurate evaluations of inter-mingled optical properties using realistic models for devices or biological systems.

Acknowledgements

854 | Chem. Soc. Rev., 2013, 42, 845–856

This journal is © The Royal Society of Chemistry 2013

References

1 R. G. Parr and W. Yang, *Density-Functional Theory of Atoms and Molecules*, Oxford University Press, New York, 1989.
2 A. D. Becke, *J. Chem. Phys.*, 1993, **98**, 5648–5652.
3 Y. Zhao and D. G. Truhlar, *Acc. Chem. Res.*, 2008, **41**, 157–167.
4 E. Runge and E. K. U. Gross, *Phys. Rev. Lett.*, 1984, **52**, 997–1000.
5 M. E. Casida, in *Time-Dependent Density-Functional Response Theory for Molecules*, ed. D. P. Chong, World Scientific, Singapore, 1995, vol. 1, pp. 155–192.
6 R. E. Stratmann, G. E. Scuseria and M. J. Frisch, *J. Chem. Phys.*, 1998, **109**, 8218–8224.
7 *Fundamentals of Time-Dependent Density Functional Theory*, ed. M. A. L. Marques, F. M. S. Nogueira, E. K. U. Gross and A. Rubio, Springer-Verlag, Heidelberg, 2012, vol. 837.
8 G. Onida, L. Reining and A. Rubio, *Rev. Mod. Phys.*, 2002, **74**, 601–659.
9 J. R. Chelikowsky, L. Kronik and I. Vasiliev, *J. Phys.: Condens. Matter*, 2003, **15**, R1517–R1547.
10 A. Rosa, D. Riccardi, O. V. Gritsenko and E. J. Baerends, *Struct. Bonding*, 2004, **112**, 49–116.
11 A. Dreuw and M. Head-Gordon, *Chem. Rev.*, 2005, **105**, 4009–4037.
12 V. Barone, R. Improta and N. Rega, *Acc. Chem. Res.*, 2008, **41**, 605–616.
13 D. Jacquemin, E. A. Perpète, I. Ciofini and C. Adamo, *Acc. Chem. Res.*, 2009, **42**, 326–334.
14 M. E. Casida, *THEOCHEM*, 2009, **914**, 3–18.
15 M. van Faasen and K. Burke, *Phys. Chem. Chem. Phys.*, 2009, **11**, 4437–4450.
16 R. Baer, L. Kronik and S. Kümmel, *Chem. Phys.*, 2011, **391**, 1–176.
17 D. Jacquemin, B. Mennucci and C. Adamo, *Phys. Chem. Chem. Phys.*, 2011, **13**, 16987–16998.
18 C. van Caillie and R. D. Amos, *Chem. Phys. Lett.*, 1999, **308**, 249–255.
19 F. Furche and R. Ahlrichs, *J. Chem. Phys.*, 2002, **117**, 7433–7447.
20 M. Dierksen and S. Grimme, *J. Phys. Chem. A*, 2004, **108**, 10225–10237.
21 L. Goerigk and S. Grimme, *J. Chem. Phys.*, 2010, **132**, 184103.
22 R. Send, M. Kühn and F. Furche, *J. Chem. Theory Comput.*, 2011, **7**, 2376–2386.
23 D. Jacquemin, A. Planchat, C. Adamo and B. Mennucci, *J. Chem. Theory Comput.*, 2012, **8**, 2359–2372.
24 J. Liu and W. Liang, *J. Chem. Phys.*, 2011, **135**, 014113.

25 S. Chibani, B. Le Guennic, A. Charaf-Eddin, O. Maury, C. Andraud and D. Jacquemin, *J. Chem. Theory Comput.*, 2012, **8**, 3303–3313.
26 F. Santoro, A. Lami, R. Improta, J. Bloino and V. Barone, *J. Chem. Phys.*, 2008, **128**, 224311.
27 D. Jacquemin, E. Brémond, I. Ciofini and C. Adamo, *J. Phys. Chem. Lett.*, 2012, **3**, 468–471.
28 V. Barone, J. Bloino, S. Monti, A. Pedone and G. Prampolini, *Phys. Chem. Chem. Phys.*, 2011, **13**, 2160–2166.
29 J. Tomasi, B. Mennucci and R. Cammi, *Chem. Rev.*, 2005, **105**, 2999–3094.
30 M. Caricato, B. Mennucci, J. Tomasi, F. Ingrosso, R. Cammi, S. Corni and G. Scalmani, *J. Chem. Phys.*, 2006, **124**, 124520.
31 R. Improta, V. Barone and F. Santoro, *Angew. Chem., Int. Ed.*, 2007, **46**, 405–408.
32 T. Vreven and K. Morokuma, *J. Comput. Chem.*, 2000, **21**, 1419–1432.
33 P. V. Parandekar, H. P. Hratchian and K. Raghavachari, *J. Chem. Phys.*, 2008, **129**, 145101.
34 A. Severo Pereira Gomes and C. R. Jacob, *Annu. Rep. Prog. Chem., Sect. C: Phys. Chem.*, 2012, **108**, 222–277.
35 D. Jacquemin, E. A. Perpète, A. D. Laurent, X. Assfeld and C. Adamo, *Phys. Chem. Chem. Phys.*, 2009, **11**, 1258–1262.
36 F. Labat, I. Ciofini, H. P. Hratchian, M. J. Frisch, K. Raghavachari and C. Adamo, *J. Am. Chem. Soc.*, 2009, **131**, 14290–14298.
37 M. E. Beck, *Int. J. Quantum Chem.*, 2005, **101**, 683–689.
38 J. Schanda, *Colorimetry: Understanding the CIE System*, Wiley, Hoboken, New Jersey, 2007.
39 T. Le Bahers, C. Adamo and I. Ciofini, *J. Chem. Theory Comput.*, 2011, **7**, 2498–2506.
40 I. Ciofini, T. Le Bahers, C. Adamo, F. Odobel and D. Jacquemin, *J. Phys. Chem. C*, 2012, **116**, 11946–11955.
41 B. Champagne, E. A. Perpète, S. van Gisbergen, E. J. Baerends, J. G. Snijders, C. Soubra-Ghaoui, K. Robins and B. Kirtman, *J. Chem. Phys.*, 1998, **109**, 10489–10498.
42 A. Dreuw and M. Head-Gordon, *J. Am. Chem. Soc.*, 2004, **126**, 4007–4016.
43 R. J. Magyar and S. Tretiak, *J. Chem. Theory Comput.*, 2007, **3**, 976–987.
44 M. J. G. Peach, P. Benfield, T. Helgaker and D. J. Tozer, *J. Chem. Phys.*, 2008, **128**, 044118.
45 A. Savin, in *Recent Developments and Applications of Modern Density Functional Theory*, ed. J. M. Seminario, Elsevier, Amsterdam, 1996, ch. 9, pp. 327–354.
46 H. Iikura, T. Tsuneda, T. Yanai and K. Hirao, *J. Chem. Phys.*, 2001, **115**, 3540–3544.
47 T. Stein, L. Kronik and R. Baer, *J. Chem. Phys.*, 2009, **131**, 244119.
48 B. M. Wong, M. Piacenza and F. Della Sala, *Phys. Chem. Chem. Phys.*, 2009, **11**, 4498–4508.
49 R. Kobayashi and R. D. Amos, *Chem. Phys. Lett.*, 2006, **420**, 106–109.
50 O. V. Gritsenko and E. J. Baerends, *J. Chem. Phys.*, 2004, **121**, 655–660.
51 P. Wiggins, J. A. Gareth Williams and D. J. Tozer, *J. Chem. Phys.*, 2009, **131**, 091101.

52 J. Plötner, D. J. Tozer and A. Dreuw, *J. Chem. Theory Comput.*, 2010, **6**, 2315–2324.

53 C. A. Guido, B. Mennucci, D. Jacquemin and C. Adamo, *Phys. Chem. Chem. Phys.*, 2010, **12**, 8016–8023.

54 R. Send, O. Valsson and C. Filippi, *J. Chem. Theory Comput.*, 2011, **7**, 444–455.

55 D. Jacquemin, Y. Zhao, R. Valero, C. Adamo, I. Ciofini and D. G. Truhlar, *J. Chem. Theory Comput.*, 2012, **8**, 1255–1259.

56 M. J. G. Peach, M. J. Williamson and D. J. Tozer, *J. Chem. Theory Comput.*, 2011, **7**, 3578–3585.

57 M. R. Silva-Junior, M. Schreiber, S. P. A. Sauer and W. Thiel, *J. Chem. Phys.*, 2008, **129**, 104103.

58 D. Jacquemin, V. Wathelet, E. A. Perpète and C. Adamo, *J. Chem. Theory Comput.*, 2009, **5**, 2420–2435.

59 R. L. Martin, *J. Chem. Phys.*, 2003, **118**, 4775–4777.

60 M. E. Casida and M. Huix-Rotllant, *Ann. Rev. Phys. Chem.*, 2012, **63**, 287–323.